Int. J. Electrochem. Sci., 9 **(2014)** 5454 - 5466

International Journal of
ELECTROCHEMICAL
SCIENCE
www.electrochemsci.org

Effect of Fluoride Ions on Oxygen Reduction and Evolution Reaction at α-MnO_2 Cathode

Imgon Hwang, Eunsaem Ahn, Yongsug Tak[*]

Department of Chemical Engineering, Inha University,253 Yonghyun-dong, Nam-ku, Incheon 402-751,Republic of Korea.
[*]E-mail: ystak@inha.ac.kr

Received: 8 May 2014 / *Accepted:* 22 June 2014 / *Published:* 16 July 2014

Development of electrode materials and electrolytes with low overpotentials during oxygen reduction reaction (discharging) and oxygen evolution reaction (charging) is essential for achieving high efficiency in aqueous Li-air batteries. α-MnO_2 was hydrothermally synthesized and used as an electrode to investigate its possible application in an aqueous Li-air battery. The electrolyte was modified by the addition of trace amounts of halide anions and alkali metal cations. Fluoride anions and potassium cations are most effective in reducing the overpotential of oxygen reduction and evolution reactions. Electrochemical studies and XPS analysis support the fact that the specific adsorption of F^- inside the double layer changes the oxidation state from Mn(IV) to Mn(III), resulting in an increase in catalytic activity for oxygen reduction/evolution reactions.

Keywords: Li-air battery, fluoride ion, oxygen reduction reaction, oxygen evolution reaction, aqueous electrolyte

1. INTRODUCTION

Rechargeable Li-air batteries have been investigated as energy storage and conversion systems because their theoretical energy storage capacity is much greater than that of Li-ion batteries [1-4]. Based on the type of electrolyte used, Li-air batteries are classified into aqueous and non-aqueous systems [5-8]. A non-aqueous system has limited cyclability because the discharge products on air cathodes are solid materials (Li_2O and Li_2O_2) that cannot be completely dissociated during the charging step. However, the aqueous Li-air battery system has an advantage over the non-aqueous system in that its soluble discharge product (OH^-) does not accumulate during cycling [8,9]. Reactions at the air electrode in an aqueous Li-air battery are considered to be an oxygen reduction reaction

(ORR) ($O_2 + 2H_2O + 4e \rightarrow 4OH^-$) during discharging and an oxygen evolution reaction (OER) ($4OH^- \rightarrow O_2 + 2H_2O + 4e$) during the charging process [10-14].

In an aqueous Li-air battery, the ORR during discharging is the same as the cathode reaction of the alkaline fuel cell, while the OER during the charging process corresponds to the anode reaction during alkaline water electrolysis. An air electrode for an aqueous Li-air battery requires high catalytic activities for both ORR and OER. Although manganese-oxide-based cathodes for ORR have been extensively studied for alkaline fuel cell and non-aqueous metal-air battery applications [15-20], their application in both ORR and OER has not yet been investigated for aqueous Li-air batteries. In addition, battery performance is not only significantly affected by the high efficiency of the air electrodes but also by electrolyte compositions.

With respect to electrolyte compositions, it has been reported that trace amounts of ions in the electrolyte expedite the rate of electrode reactions by either electrostatic effects or ligand-bridged electron-transfer pathways [21]. In the Cu-deposition process, the Cu^{2+}/Cu^+ reaction is catalyzed by chloride ions through a chloride-ion-bridged inner sphere reaction [21]. More recently, the effect of solution additives on electrode activity has been reported for the hydrogen evolution reaction (HER), $2H_2O + 2e \rightarrow H_2 + 2OH^-$, in alkaline water electrolysis. Either Li^+ or Ba^{2+} reduces the HER overpotential by forming an adsorbed state that suppresses the access of gas molecules, such as O_2 and H_2, to the electrode surface [22]. These cations play a role in increasing the effective surface area, and ultimately, improving cathode efficiency. Therefore, it can be suggested that specifically adsorbed ions inside the inner Helmholtz layer of an electrode/electrolyte interface may catalyze the ORR and OER in aqueous Li-air batteries.

In this study, we investigated the effect of trace amounts of different ionic species on the ORR and OER for a hydrothermally prepared α-MnO_2 electrode in KOH solution. Reaction pathway and the catalytic activity of α-MnO_2 were investigated with linear sweep voltammetry (LSV) and Koutecky-Levich analysis.

2. EXPERIMENTAL

An α-MnO_2 electrode was prepared by the hydrothermal method. 2 mmol $KMnO_4$ and 1 mL H_2SO_4 were dissolved in 20 mL of deionized water and maintained at 150℃ for 12 h in an autoclave [23]. 1M KOH was used as the main electrolyte for the aqueous Li- O_2 batteries and trace amounts of anions in the form of KF, KCl, and KI were added to the 1 M KOH solution to investigate the effect of anions on the ORR and OER. The electrochemical behavior of ORR on α-MnO_2 was investigated with a potentiostat (Autolab PGSTAT302N) and a rotating disc electrode system (RDE, Autolab). The working electrode, α-MnO_2, on the RDE system was prepared using the following procedure: a mixture of water, α-MnO_2, and nafion solution were homogeneously stirred for 1 h in an ultrasonic bath, following which, 3 μL of this mixture was poured over the surface of a glassy carbon electrode (GCE, 0.071 cm^2) and dried overnight in air at room temperature. Pt foil and Hg/HgO/1M NaOH were used as the counter electrode and reference electrode, respectively. The potential for ORR was varied

from 0.3 to - 0.5 V vs. Hg/HgO/1M NaOH at a scan rate of 20 mV/s and the rotating speed was fixed at 4000 rpm.

The structure of the α-MnO_2 electrode was analyzed with an X-ray diffractometer (XRD) (Rigaku, D/Max-2200) and its surface elemental composition was investigated with X-ray photoelectron spectroscopy (XPS, ULVAC-PHI) using monochromated Al Kα radiation (*hv* is 1486.6 eV).

3. RESULTS AND DISCUSSION

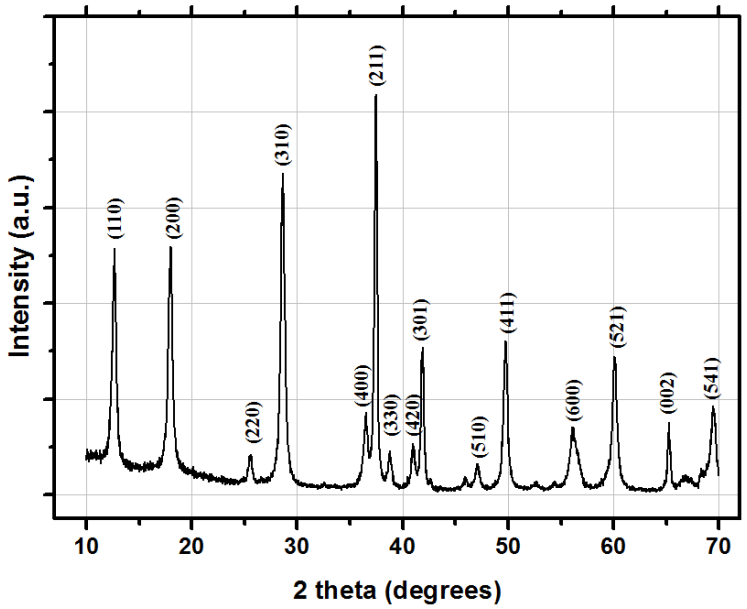

Figure 1. XRD of the α-MnO_2 electrode synthesized using a hydrothermal method.

Fig. 1 shows the structure of the α-MnO_2 electrode prepared by using a hydrothermal method; the XRD peaks are indexed to a body-centered tetragonal α-MnO_2 phase [24]. Fig. 2 shows that the α-MnO_2 electrode has a low catalytic activity for $H_2O + 2e \rightarrow H_2 + 2OH$ in the absence of dissolved O_2, but a high catalytic activity for $O_2 + 2H_2O + 4e \rightarrow 4OH^-$ in an O_2-saturated 1M KOH. To investigate the effect of halide anions on the ORR in an O_2-saturated solution, 0.001 M of KF, KCl, and KI were added to 1 M KOH to alleviate the cation effects on the ORR. The linear sweep voltammogram of Fig. 3 indicates that the addition of Cl^- and I^- ions suppressed the ORR but that the F^- ions favored he rate of ORR. In order to elucidate the effect of F^- on ORR, different concentrations of F^- ions, from 0.001M to 0.01 M, were prepared and tested by LSV. Fig. 4 shows that the F^- ion affected the ORR significantly. Catalytic activity of α-MnO_2 increases at concentrations below 0.006M F^-, but it decreases above 0.008 M F^-. At a potential of -0.25 V vs. Hg/HgO/1M NaOH, the cathodic current density was -2.13 mA/cm^2 in the absence of F^- ions, and it reached -2.17 mA/cm^2 at 0.001 M F^-; -2.45 mA/cm^2 at 0.002 M F^-; -3.48 mA/cm^2 at 0.004 M F^-; and -2.69 mA/cm^2 at 0.006 M F^-. The highest

charge transfer rate and the lowest initial reduction potential, E_i, for the ORR were observed after the addition of 0.004 M F^- in 1M KOH.

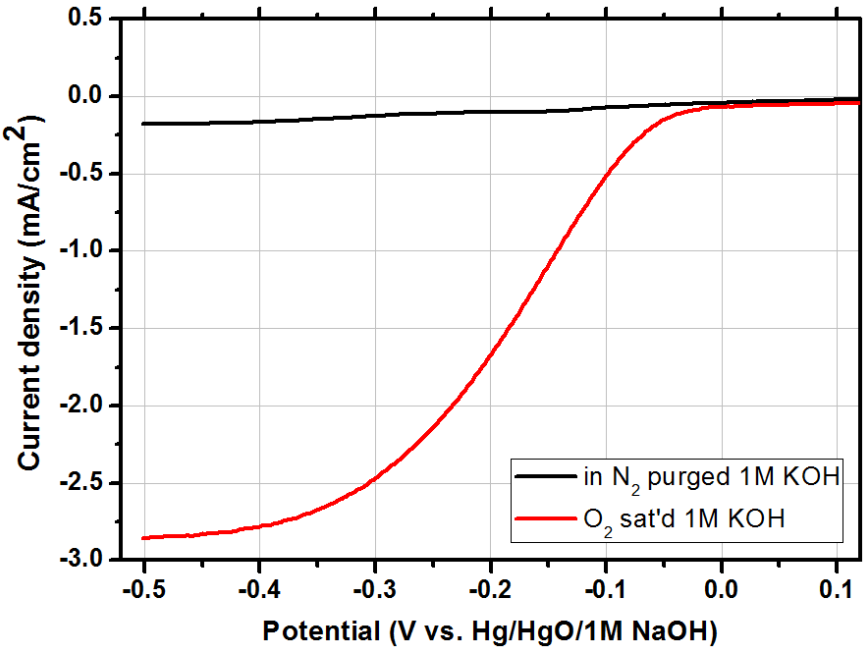

Figure 2. Polarization curves for the oxygen reduction reaction at the α-MnO_2 cathode in 1 M KOH with a N_2 purged and an O_2 saturated environment. scan rate: 20 mV/s, rotation speed: 4000 rpm.

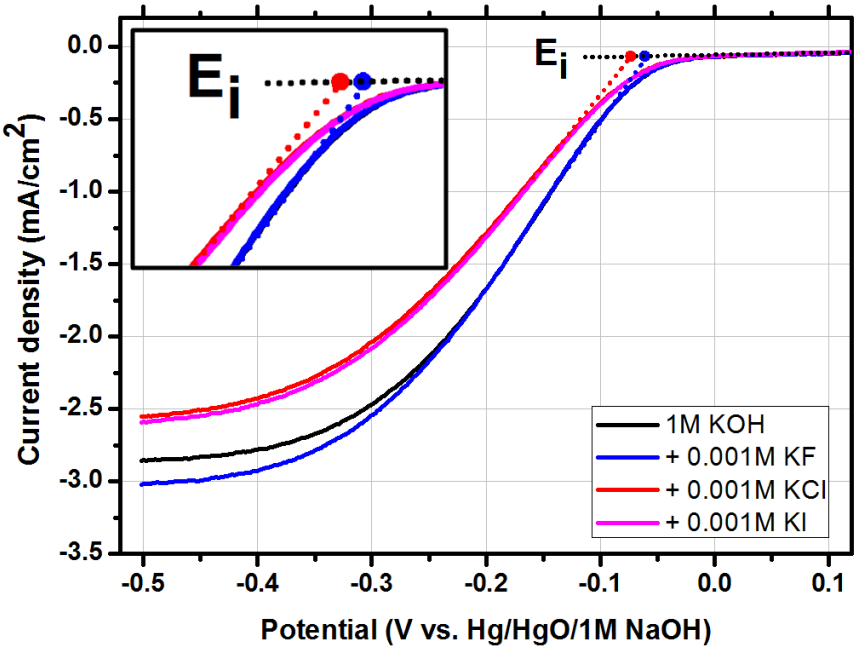

Figure 3. Polarization curves for the oxygen reduction reaction at the α-MnO_2 cathode in pure 1 M KOH and 1 M KOH containing 0.001 M of KCl, KF, and KI. scan rate: 20 mV/s; rotation speed 4000 rpm.

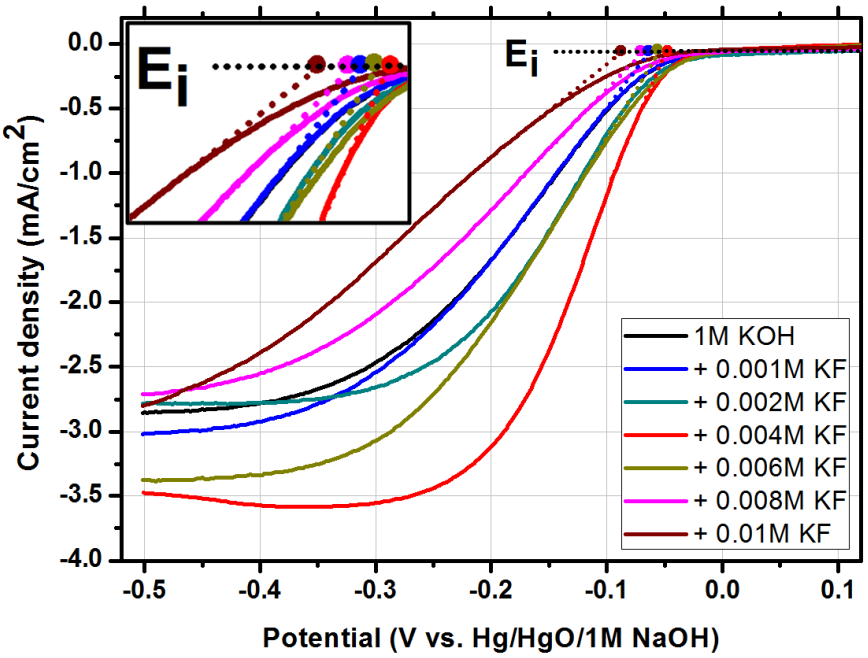

Figure 4. Polarization curves for the oxygen reduction reaction at the α-MnO_2 cathode in pure 1 M KOH and 1 M KOH containing different amounts of KF. scan rate: 20 mV/s; rotation speed: 4000 rpm.

Polarization curves of ORR with oxygen saturated 1M KOH solution was rapidly decreased below -0.02 V (vs. Hg/HgO/1M NaOH), while 1M KOH with nitrogen purged solution cannot appeared ORR activity of α-MnO_2 cathode. It can prove that oxygen within solution was reduced rather than α-MnO_2 catalyst. In order to investigate the effect of halide anions on the ORR at the α-MnO_2 cathode, a linear sweep voltammogram was measured with the addition of 0.001 M KF, KCl, and KI in 1 M KOH. Fig. 3 indicates that the addition of a small amount of Cl^- and I^- ions generates the high overpotential for the initiation of the ORR and also increases the fast charge transfer rate below -0.25 V (vs. Hg/HgO/1M NaOH). Unlike the Cl^- and I^- ions, the presence of F^- ions increased the rate of the ORR within the entire scan range of potentials by substantially increasing the catalytic activity of the α-MnO_2 cathode. The NO_3^- ions show an effect similar to that of the ORR with Cl^- and I^- ions.

In order to elucidate the effect of F^- ions on the ORR at the α-MnO_2 cathode, polarization data at different rotation speeds and electrode potentials were exploited to plot the Koutecky-Levich (K-L) equation. The number of electrons (n) participating in the ORR was obtained from the slopes of the K-L curves [25]:

$$i^{-1} = i_k^{-1} + i_L^{-1} = (nFkC_o)^{-1} + (0.62nFD^{2/3}C_o\nu^{-1/6}\omega^{1/2})^{-1}$$

where i is the measured current density, i_k and i_L are the kinetic- and diffusion-limiting current densities, respectively, F is the Faraday constant (96,485 C/mol), A is the geometric area of the RDE, D is the diffusion coefficient of O_2 in 1 M KOH (1.76×10^{-5} cm^2/s), C_o is the concentration of O_2 in 1 M KOH at 25 °C (1.103×10^{-6} mol/cm^3), ν is the kinematic viscosity (0.01 cm^2/s), ω is the angular velocity of the electrode, and k is the electron transfer rate constant. Fig. 5(a) and 5(b) show the K-L plots (i^{-1} vs. $\omega^{-1/2}$) corresponding to the 1 M KOH and the 1 M KOH containing 0.004 M KF,

respectively. The n value of the ORR was 2.50 in 1 M KOH and increased to 2.98 in the 0.004M KF-containing KOH solution.

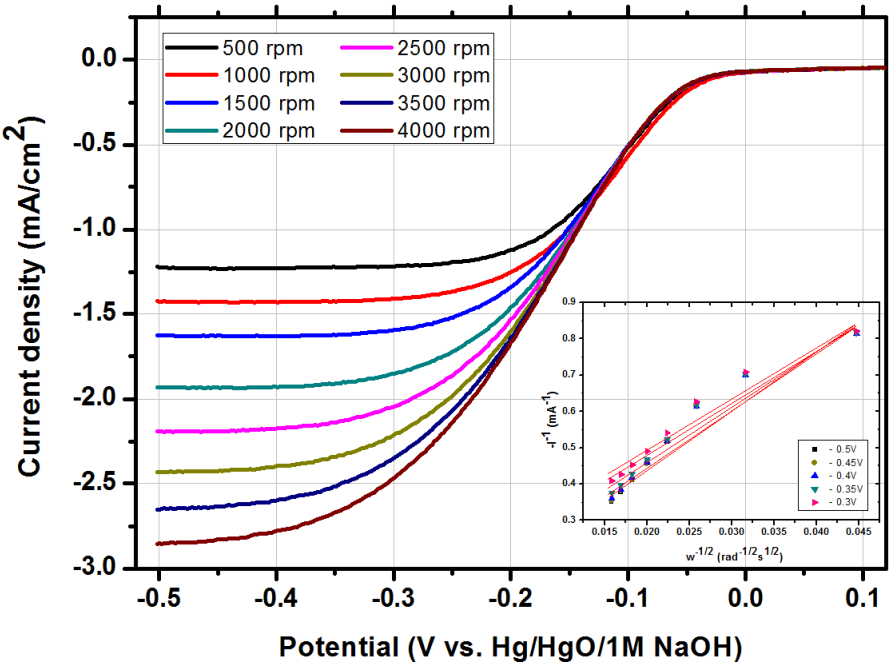

A

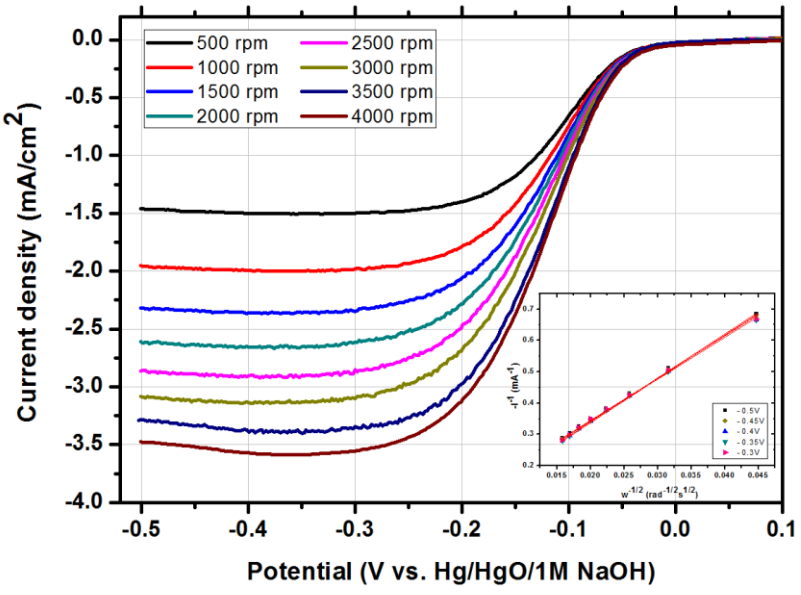

B

Figure 5. Polarization curves and Koutecky-Levich plot for the oxygen reduction reaction at the cathode in (a) 1 M KOH only and (b) 1 M KOH containing 0.004 M KF. scan rate: 20 mV/s; rotation speed: 4000 rpm.

The exchange current density (i_o) was obtained from the Tafel plot using the following equation:

$$\log i_K = \log i_o + (1-\alpha)nF\eta/2.303RT$$

i_o was 6.74×10^{-3} A/cm^2 in 1 M KOH and 1.85×10^{-2} A/cm^2 in the 1 M KOH containing 0.004 M KF. The exchange current density in the presence of 0.004M F^- was three times higher than that in the pure 1 M KOH. Table 1 shows the initial reduction potential and exchange current density in different solution compositions.

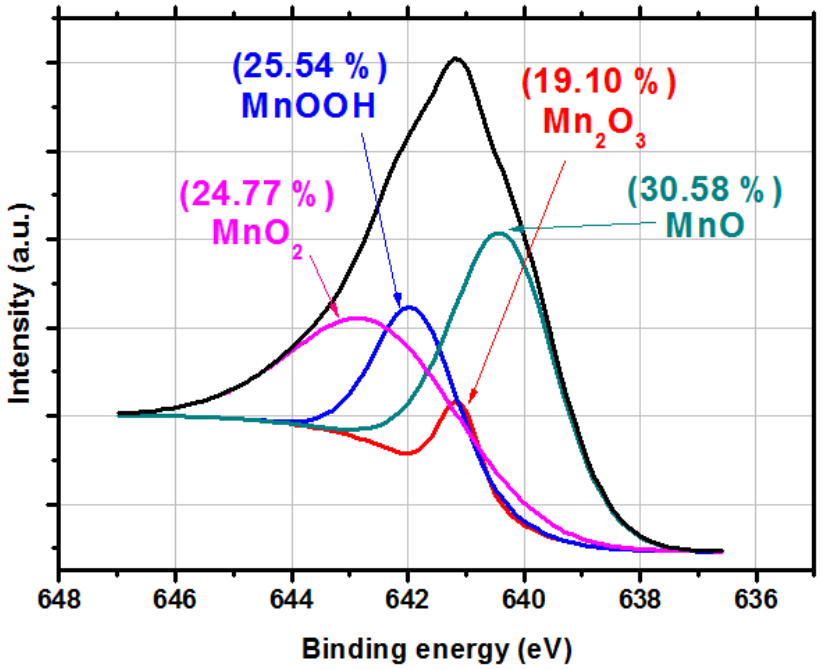

A

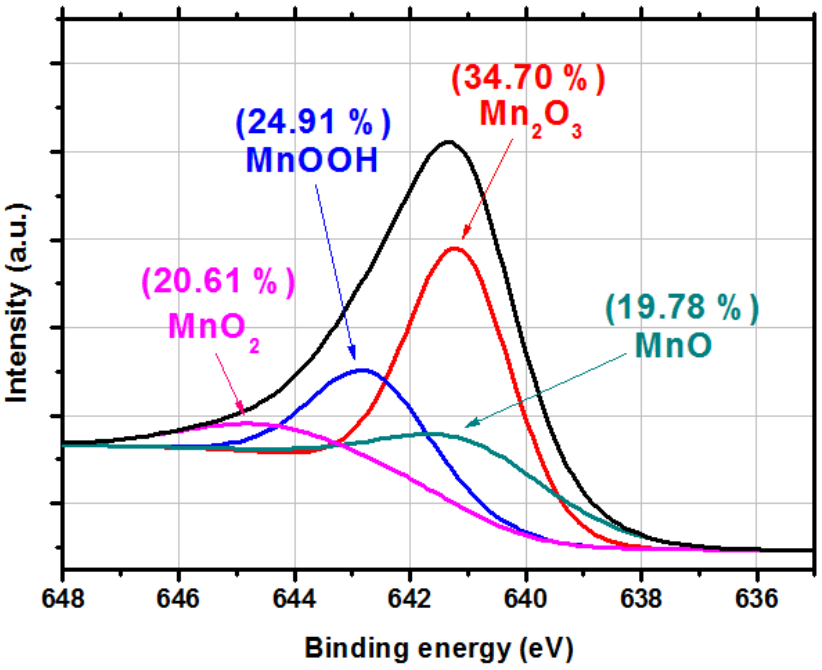

B

Figure 6. XPS $Mn_{2p3/2}$ spectra of the α-MnO_2 cathode after the oxygen reduction reaction in (a) 1M KOH only and (b) 1M KOH containing 0.004M KF. The oxygen reduction reactions were tested by linear sweep voltammetry. scan rate: 20 mV/s; rotation speed: 4000 rpm.

Table 1. Initial reduction potential, E_i, and exchange current density for the oxygen reduction reaction at the α-MnO_2 cathode in different compositions of the electrolyte.

Electrolyte composition	Initial reduction potential, E_i (V vs. Hg/HgO/1M NaOH)	i_o (A/cm^2)
1 M KOH	-0.058	6.74×10^{-3}
0.002 M KF*	-0.052	7.38×10^{-3}
0.004 M KF*	-0.048	1.85×10^{-2}
0.006 M KF*	-0.052	8.83×10^{-3}
0.008 M KF*	-0.071	1.80×10^{-3}
0.01 M KF*	-0.093	1.62×10^{-3}

* Specific concentration of KF is added in 1 M KOH.

The ORR at α-MnO_2 was assumed to proceed via a mixed two-electron and four-electron pathway in the aforementioned electrolytes, pure KOH, and KOH containing KF. The reaction $O_2 + H_2O + 2e \rightarrow HO_2^- + OH^-$ involved a two-electron pathway, whereas the ORR entailed a four-electron pathway when the following disproportionation reaction ended: $2HO_2^- \rightarrow O_2 + 2OH^-$. Lima et al. asserted that the change in oxidation state from Mn(IV) to Mn(III) was responsible for the higher catalytic activity for ORR [26]. Mn(III) might have existed as Mn_2O_3, which was eventually converted into MnOOH. However, the effect of a trace amount of F^- ions on the oxidation state of Mn(IV) has never been investigated and still remains unclear. Since MnO_2 is known to be a good adsorbent of arsenic and fluoride ions in water [26,27], it can be supposed that F^- ions are adsorbed onto the surface of α-MnO_2. Assuming an electric double layer structure on a negatively charged electrode [28], F^- anions can be specifically adsorbed inside an inner Helmholtz layer. In order to investigate the existence of Mn(III) species during ORR in 1 M KOH containing 0.004 M F^- solution, the $Mn_{2p3/2}$ peak of the α-MnO_2 cathode was analyzed with XPS after the ORR in the pure 1M KOH and 1 M KOH with 0.004 M KF solutions. Fig. 6 shows that the proportion of Mn(III) components, such as MnOOH and Mn_2O_3, clearly increased in the 1 M KOH containing the 0.004 M KF electrolyte (Fig. 6(b), 59.61 %), as compared with the pure 1M KOH (Fig. 6(a), 44.64 %). This indicates that the adsorption of trace amounts of F^- onto an α-MnO_2 cathode may transfer electrons to α-MnO_2 and change the oxidation state of Mn(IV) to Mn(III), thereby increasing the catalytic activity for the ORR. However, the cause for the decrease in catalytic behavior of α-MnO_2 above 0.008M F^- is still unclear.

With fixed concentration of the fluoride anion (0.004 M), which had the highest catalytic effect on the ORR, different types of monovalent cations were tested in the form of LiF, NaF, and KF in 1 M KOH. The corresponding linear sweep voltammograms for each cation in separate solutions are shown in Fig. 7. Table 2 shows the initiation potential and exchange current density (i_o) for the ORR. With the addition of LiF, NaF, and KF, the initiation potential for the ORR decreased and the catalytic activity of the electrode increased sharply, as indicated by the increase in the value of the exchange current density in Table 2. At a potential of -0.25 V(vs. Hg/HgO/1M NaOH), the cathodic current density was

-2.13 mA/cm^2 in 1 M KOH, but it can be verified -1.48 mA/cm^2 at 0.004 M Li^+, -1.50 mA/cm^2 at 0.004 M Na^+, and -3.48 mA/cm^2 at 0.004 M K^+ containing 1M KOH solutions, respectively.

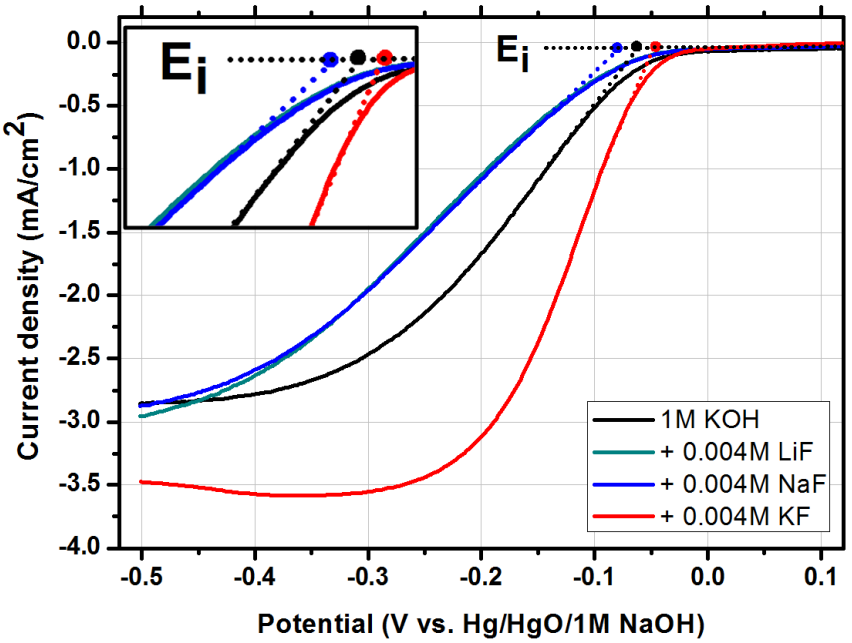

Figure 7. Polarization curves for the oxygen reduction reaction at the α-MnO_2 cathode in pure 1 M KOH and 1 M KOH containing 0.004 M of LiF, NaF, and KF. scan rate: 20 mV/s; rotation speed: 4000 rpm.

The KF-containing electrolyte had the highest catalytic effect on the ORR, while the LiF and NaF-containing electrolyte had the lowest catalytic activity rather than 1M KOH solution. The radii of the hydrated cations decreased in the order, $K^+ < Na^+ < Li^+$, because of ion-water solvent interactions [17]. Therefore, it can be inferred that the hydrated cations are adsorbed onto the outer Helmholtz layer inside the electric double layer structure and thereby inhibit the adsorption of dissolved O_2 at the electrode surface, which can decrease the rate of the ORR. Therefore, the least hydrated alkali metal ion, K^+, showed the highest catalytic activity for the ORR in the presence of 0.004 M fluoride ion.

Table 2. Initial reduction potential, E_i, and exchange current density for the oxygen reduction reaction at the α-MnO_2 cathode in different compositions of the electrolyte.

Electrolyte composition	**Initial reduction potential, E_i (V vs. Hg/HgO/1M NaOH)**	**i_o (A/cm^2)**
1 M KOH	-0.058	6.74×10^{-3}
0.004 M LiF*	-0.072	4.78×10^{-3}
0.004 M NaF*	-0.072	4.87×10^{-3}
0.004 M KF*	-0.048	1.85×10^{-2}

* LiF, NaF, and KF are added in 1 M KOH.

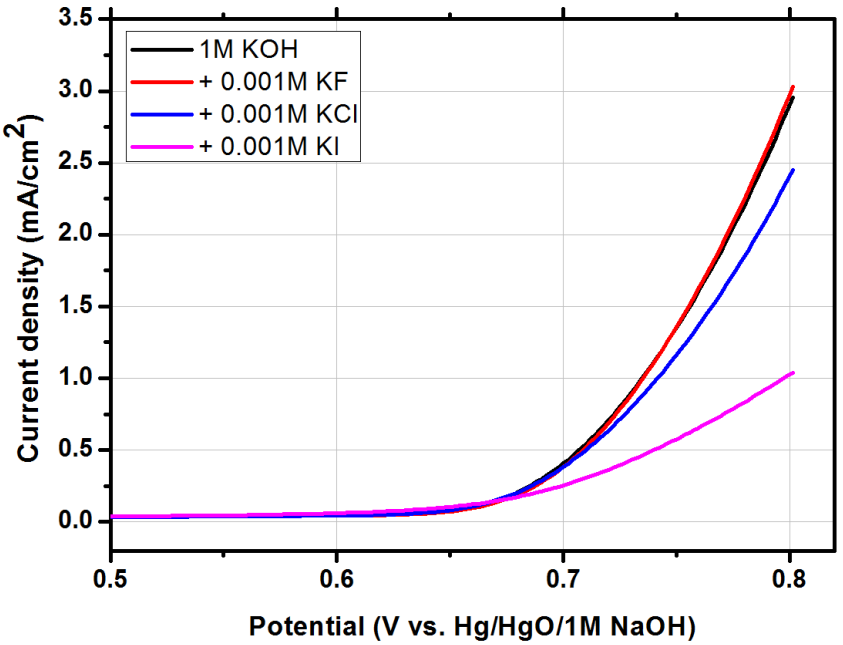

Figure 8. Polarization curves for the oxygen evolution reaction at the α-MnO_2 anode in pure 1 M KOH and 1 M KOH containing 0.001 M of KCl, KF, and KI. scan rate: 20 mV/s; rotation speed: 4000 rpm.

In order for α-MnO_2 to be applied for aqueous Li-O_2 battery, it should have a high catalytic activity for oxygen evolution reaction, which is the reaction during battery charging. Effect of α-MnO_2 electrode on oxygen evolution reaction was investigated in different compositions of electrolyte and linear sweep voltammetry was carried out by adding 0.001 M KF, KCl, KI in 1M KOH, following the same procedure for ORR.

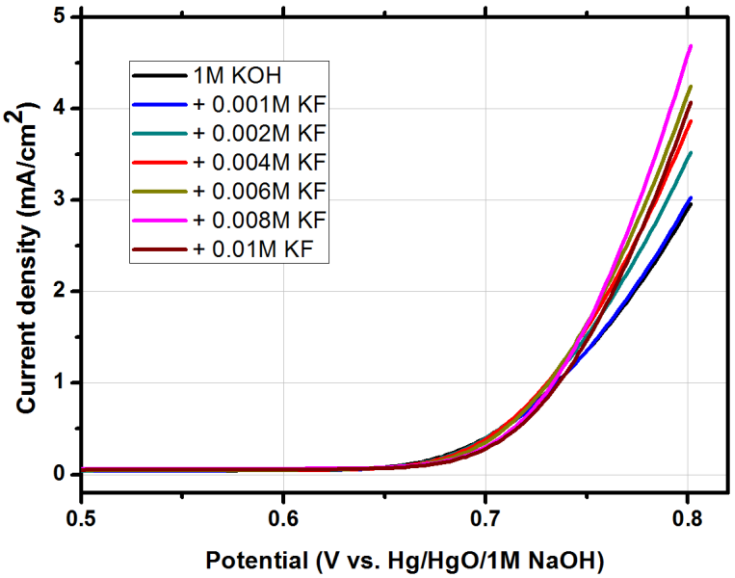

Figure 9. Polarization curves for the oxygen evolution reaction at the α-MnO_2 anode in pure 1 M KOH and 1 M KOH containing different amounts of KF. scan rate: 20 mV/s; rotation speed 4000 rpm.

Table 3. Exchange current density for the oxygen evolution reaction at the α-MnO_2 anode in different compositions of the electrolyte.

Electrolyte composition	i_o (A/cm^2)
1 M KOH	2.60×10^{-3}
0.002 M KF	2.66×10^{-3}
0.004 M KF	2.85×10^{-3}
0.006 M KF	3.39×10^{-3}
0.008 M KF	4.17×10^{-3}
0.01 M KF	2.95×10^{-3}

* Specific concentration of KF is added in 1 M KOH.

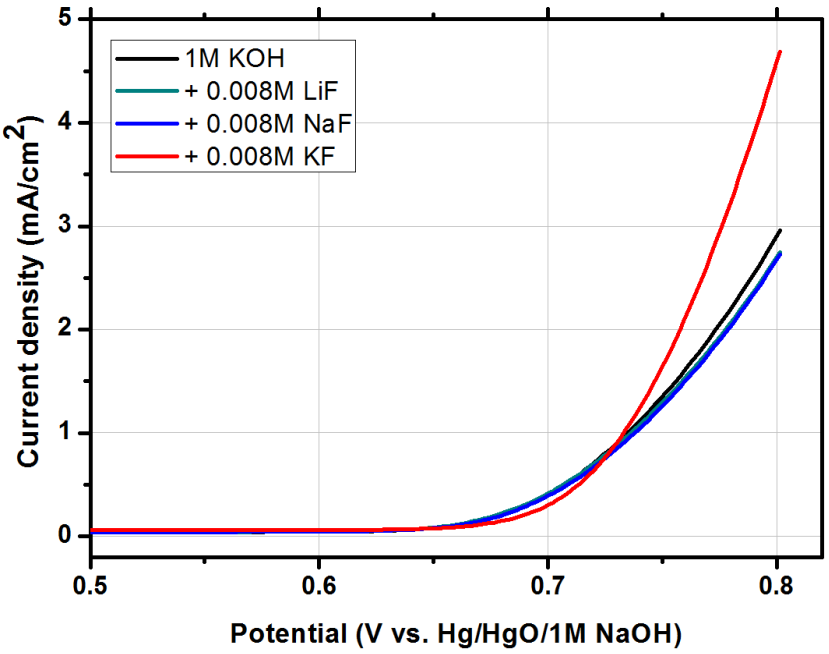

Figure 10. Polarization curves for the oxygen evolution reaction at the α-MnO_2 anode in pure 1 M KOH and 1 M KOH containing 0.008 M of LiF, NaF, and KF. scan rate: 20 mV/s; rotation speed 4000 rpm.

Fig. 8 indicates that addition of 0.001M of F^- ion did not affect the OER catalytic activity of α-MnO_2 but Cl^-, I^- suppressed OER. Linear sweep voltammogram of Fig. 9 shows that the activity of α-MnO_2 for OER was gradually increased up to 0.008M of F^- as the concentration of F^- increases. Table 3 shows that exchange current density, i_o, for OER was 2.60×10^{-3} A/cm^2 in 1 M KOH and 4.17×10^{-3} A/cm^2 in the 1 M KOH containing 0.008 M F^-. With the same reasoning for oxygen reduction reaction, it can be suggested that oxidation state change from Mn(IV) to Mn(III) of α-MnO_2 by the adsorption of F^- affects the charge transfer rate of oxygen evolution reaction. Fig. 10 shows the effects of different cation species, LiF, NaF, and KF, on OER in the presence of 0.008M F^-. As indicated in Table 4, KF shows the highest catalytic activity and highest exchange current density. This observation can be

explained by the adsorption of smallest hydrated cation of K^+ on α-MnO_2, as suggested in the discussion of oxygen reduction reaction.

Table 4. Exchange current density for the oxygen evolution reaction at the α-MnO_2 anode in different compositions of the electrolyte.

Electrolyte composition	i_o (A/cm^2)
1 M KOH	2.60×10^{-3}
0.008 M LiF	2.91×10^{-3}
0.008 M NaF	3.05×10^{-3}
0.008 M KF	4.17×10^{-3}

* LiF, NaF, and KF are added in 1 M KOH.

4. CONCLUSION

Oxygen electrodes of aqueous Li- O_2 batteries should have superior catalytic activities for ORR during discharging and OER during the charging process. In this work, the effects of electrolyte compositions on the ORR and OER on a hydrothermally prepared α-MnO_2 electrode were investigated using an electrochemical method and XPS analysis. The presence of 1 M KOH containing 0.004M F^- catalyzed the ORR significantly, resulting in an exchange current density 2.7 times higher than that observed with pure 1M KOH. Electrochemical analysis and XPS results suggest that specifically adsorbed F^- is responsible for the fast charge transfer rate for ORR by changing the oxidation state of Mn(IV) to Mn(III) in α-MnO_2. The observed higher activity of KF compared to that of NaF and LiF with the same 0.004M F^- can be explained by the difference in the size of hydrated cations. In addition, fluoride anions have a catalytic effect for the OER and 0.008M F^- in 1M KOH has an exchange current density 1.6 times higher than that of pure 1M KOH. However, the other anions, Cl^- and I^-, have negative catalytic effects on both ORR and OER at α-MnO_2 electrodes. These results suggest that F^- in the form of KF is a very effective additive in reducing the overpotential for the ORR and OER at α-MnO_2 electrodes.

ACKNOWLEDGEMENT
This work was supported by the National Research Foundation of Korea Grant Funded by the Korean Government (MEST) (NRF-2012-M1A2A2671765) and the INHA UNIVERSITY Research Grant.

References

1. A. Debart, A. Paterson, M. Holzapfel, P. Bruce, *Angew. Chem., Int. Ed,*. 47 (2008) 4521.
2. R. Black, S. H. Oh, J. H. Lee, T. Yim, B. Adams, L. F. Nazar, *J. Am. Chem. Soc.*, 134 (2012) 2902.
3. X. H. Yang, P. He, Y.-Y. Xia, *Electrochem. Commum.*, 11 (2009) 1127.
4. Y. Wang, H. Zhou, *J. Power Sources*, 195 (2010) 358.

5. C. Tran, X.-Q. Yang, D. Qu, *J. Power Sources*, 195 (2010) 2057.
6. T. Zhang, N. Imanishi, S. hasegawa, A. Hirano, J. Xie, Y. Takeda, O. Yamamoto, N. Sammes, *J. Electrochem. Soc.*, 155 (2008) A965.
7. X. H. Yang, P. He, Y. Y. Xia, *Electrochem. Commun.*, 11 (2009) 1127.
8. S. Hasegawa, N. Imanishi, T. Chang, J. Xie, A. Hirano, Y. Takeda, O. Yamamoto, *J. Power Sources*, 189 (2009) 371.
9. J. Read, *J. Electrochem. Soc.*, 149 (2002) A1190.
10. Z. P. Zheng, R. Y. Liang, M. Hendrickson, E. J. Plichta, *J. Electrochem. Soc.*, 155 (2008) A432.
11. G. Girishkumar, B. McCloskey, A. C. Luntz, S. Swanson, W. Wilcke, *J. Phys. Chem. Lett.*, 1 (2010) 2193.
12. P. He, Y. Wang, H. Zhou, *Electrochem. Commun.*, 12 (2010) 1686.
13. Y. Lu, J. B. Gddoenough, Y. Kim, *J. Am. Chem. Soc.*, 133 (2011) 5756.
14. Christensen, R. Leidtke, J. Ahmed, A. Kojic, *J. Electrochem. Soc.*, 159 (2012) R1.
15. F. H. B. Lima, M. L. Calegaro, E. A. Ticianelli, *J. Electroanal. Chem.*, 590 (2006) 152.
16. I. Roche, E. Chaninet, M. Chatenet, J. Vondrak, *J. Appl. Electrochem.*, 38 (2008) 1195.
17. J. Feng, Y. Liang, H. Wang, Y. Li, B. Zhang, J. Zhou, J. Wang, T. Regier, H. Dai, *Nano Res.*, 5 (2012) 718.
18. Y. Gorlin, B. L. Kaiser, J. D. Benck, S. Gul, S. M. Webb, V. K. Yachandra, J. Yano, T. F. Jaramillo, *J. Am. Chem. Soc.*, 135 (2013) 8525.
19. A. K. Thapa, T. Ishihara, *J. Power sources*, 196 (2011) 7016.
20. T. Ogasawara, A. Debart, M. Holfazel, P. Novak, P. G. Bruce, *J. Am. Chem. Soc.*, 128 (2006) 1390.
21. Z. Nagy, J. P. Blaudeau, N. C. Hung, L. A. Curtiss, J. J. Zurawski, *J. Electrochem. Soc.*, 142 (1995) L87.
22. D. Strmcnik, D. F. van der Vliet, K. C. Chang, V. Komanicky, K. Kodama, H. You, V. R. Stamenkovic, N. M. Markovic, *J. Phys. Chem. Lett.*, 2 (2011) 2733.
23. X. Wang, Y. Li, *J. Am. Chem. Soc.*, 124 (2002) 2880.
24. K. J. Babu, A. Zahoor, K. Nahm, R. Ramachandran, M. A. J. Rajan, G. G. Kumar, *J. Nanopart. Res.*, 16 (2014) 2250.
25. F. H. B. Lima, M. L. Calegaro, E. A. Ticianelli, *Electrochim. Acta*, 52 (2007) 3732.
26. L. Batistella, L. Venquiaruto, M. D. Luccio, J. V. Dliveira, S. B. C. Pergher, M. A. Mazutti, D. D. Olivera, A. J. Mossi, H. Treichel, R. Dallgo, *Ind. Eng. Chem. Res.*, 50 (2011) 6871.
27. H. S. Kong, W. Li, H. B. Lin, Z. Shi, Y. Y. Lu, Y. Y. Dan, W. M. Huang, *Surf. Interface Anal.*, 45 (2013) 715.
28. D. C. Grahame, R. Parsons, *J. Am. Chem. Soc.*, 83 (1961) 1291.